Check for updates

Development of a small molecule-based two-photon photosensitizer for targeting cancer cells†

Dong Joon Lee,‡[a] Yu Cao, [ID] ‡[b] Vinayak Juvekar,‡[a] Sauraj,‡[a] Choong-Kyun Noh,[c] Sung Jae Shin,*[c] Zhihong Liu [ID] *[b] and Hwan Myung Kim [ID] *[a]

Photodynamic therapy (PDT) employing two-photon (TP) excitation is increasingly recognized to induce cell damage selectively in targeted areas, underscoring the importance of developing TP photosensitizers (TP-PSs). In this study, we developed **BSe-B**, a novel PS that combines a selenium containing dye with biotin, a cancer-selective ligand, and is optimized for TP excitation. **BSe-B** demonstrated enhanced cancer selectivity, efficient generation of type-I based reactive oxygen species (ROS), low dark toxicity, and excellent cell-staining capability. Evaluation across diverse cell lines (HeLa, A549, OVCAR-3, WI-38, and L-929) demonstrated that **BSe-B** differentiated and targeted cancer cells while sparing normal cells. **BSe-B** displayed excellent *in vivo* biocompatibility. In cancer models such as three-dimensional spheroids and actual colon cancer tissues, **BSe-B** selectively induced ROS production and cell death under TP irradiation, demonstrating precise spatial control. These findings highlight the potential of **BSe-B** for imaging-guided PDT and its capability for micro treatment within tissues. Thus, **BSe-B** demonstrates robust TP-PDT capabilities, making it a promising dual-purpose tool for cancer diagnosis and treatment.

Introduction

Photodynamic therapy (PDT) for cancer stands out for its reduced side effects, noninvasiveness, and site-specific treatment capabilities, distinguishing it from traditional cancer therapies such as surgery and chemotherapy.[1–4] PDT employs photosensitizers (PSs) activated by light, which interact with oxygen or biological substrates to generate cytotoxic singlet oxygen ($^1O_2$) or reactive oxygen species (ROS), thereby inducing cell damage and death.[5–10] However, clinically approved PSs such as chlorine, porphyrin, and phthalocyanine are effective primarily for superficial diseases, such as skin cancer, due to their limited tissue penetration under ultraviolet-visible (UV-Vis) light (<700 nm).[11,12] In addition, they have disadvantages, including limitations in intravenous administration owing to low solubility and lack of cancer-selective ability.[13–15] To overcome these limitations, researchers are developing PSs with enhanced cancer-targeting capabilities.

Cancer-selective ligands are gaining attention in diagnosis and treatment, playing a critical role in selectively delivering PSs to cancer cells.[16,17] Cancer cells often overexpress various tumor-specific receptors, including certain vitamin receptors that promote rapid growth, proliferation, and cell survival.[18–20] For example, receptors for biotin (vitamin B7) are notably overexpressed on the surface of cancer cells found in cervical cancer, lung cancer, breast cancer, and colon cancer.[19,21–24] Several PSs have significantly improved cancer selectivity by utilizing biotin as a targeting ligand.[25–27] Therefore, leveraging biotin as a targeting ligand to deliver PSs to cancer cells represents a promising PDT strategy toward enhancing treatment efficacy while minimizing off-target effects.

Furthermore, PDT can benefit significantly from advancements in imaging technology. Fluorescence imaging plays a crucial role in visualizing cellular and molecular processes within living organisms and offers real-time insights into various physiological and pathological conditions. However, most PDT agents lack imaging capabilities. Combining imaging ability with cancer-targeting PSs could revolutionize imaging-guided therapies, enabling precise treatment guidance and therapeutic outcome assessment. Furthermore, the integration of two-photon excitation (TPE) offers advantages over traditional UV-Vis excitation by employing longer-wavelength near-infrared (NIR) light, which penetrates more deep into tissues with reduced photodamage.[28–32] The nonlinear characteristics of TPE confine PS activation to precise locations,

[a] *Department of Energy Systems Research and Department of Chemistry, Ajou University, Suwon 16499, Korea. E-mail: kimhm@ajou.ac.kr*

[b] *College of Health Science and Engineering, Hubei University, Wuhan 430062, China. E-mail: zhhliu@whu.edu.cn*

[c] *Department of Gastroenterology, Ajou University School of Medicine, Suwon 16499, Korea. E-mail: shsj9128@ajou.ac.kr*

† Electronic supplementary information (ESI) available. See DOI: https://doi.org/10.1039/d4tb01706d

‡ Contributed equally to this work.

12232 | *J. Mater. Chem. B*, 2024, **12**, 12232–12238

This journal is © The Royal Society of Chemistry 2024

minimizing collateral damage to healthy tissues and facilitating micro treatment within tissues.[33–36] The development of PSs optimized for TPE conditions (TP-PSs) represents a promising frontier in PDT research, addressing current limitations and expanding the scope of PDT applications in clinical settings.

Small molecule-based dyes (such as fluorescent probes and PS) are easy to synthesize, allowing for various applications and modifications. They are also suitable for application to biological samples owing to their excellent staining ability on cells.[37–39] We recently reported on a dimethylaminonaphthalene (DAN) scaffold featuring an electron push–pull system, which has been used to design various two-photon fluorescent probes.[40] These dyes exhibit significant two-photon excitation, primarily due to their efficient internal charge transfer (ICT) characteristics. Herein, we performed a simple chemical modification of the DAN structure by incorporating selenium, resulting in **BSe-B** (Fig. 1a). **BSe-B** includes a cancer-targeting unit (biotin) known for its high tumor affinity and low molecular weight.[41,42] We explored the cancer selectivity and therapeutic efficacy of **BSe-B** in various cancer models, including different cell lines and tissues. Although several two-photon photosensitizers are based on small molecules (Table S1 and Scheme S2, ESI†), there have been no reports of selenium-containing, small molecule-based two-photon excited photosensitizers that target cancer cells and generate reactive oxygen species through type-I process. Incorporating imaging capabilities into PDT agents, such as **BSe-B**, not only facilitates precise treatment guidance but also enables real-time monitoring of therapeutic responses. This integration represents a significant advancement, potentially improving PDT treatment outcomes while minimizing off-target effects.

Results and discussion

Synthetic strategy and design of BSe-B

BSe-B is composed of **BSe** (TP-PS) conjugated to oligomeric ethylene glycol (a hydrophilic linker) and biotin (a cancer-targeting unit) (Fig. 1). We conjugated a hydrophilic linker in the middle to avoid affecting the ROS generation efficiency of **BSe** and the cancer selectivity of biotin. **BSe-B** can be easily modified to exploit the advantages of small-molecule dyes. First, a hydrophilic linker and biotin are conjugated to a 6-(methylamino)-2-naphthaldehyde structure using an amide-coupling reagent. Cyclization was then performed using bis(2-aminophenyl)diselenide and an acid catalyst. Consequently, we obtained **BSe-B** in a few simple steps (Scheme S1, ESI†). The **BSe-B** structure was confirmed using ^{1}H-NMR, ^{13}C-NMR, and high-resolution mass spectrometry. The detailed synthesis steps are provided in ESI.†

Photophysical characteristics and ROS generation ability of BSe-B

The photophysical characteristics of **BSe-B** were determined in each solvent (Fig. S1 and Table S2, ESI†). A maximum absorption wavelength of 370 nm and a maximum emission wavelength of 487 nm were observed. The absorption and emission spectra of **BSe-B** are red-shifted compared to the sulfur-containing BTDAN dye (Table S2, ESI†), which may be attributed to the enhanced internal charge transfer character. The fluorescence quantum yield (Φ) of **BSe-B** was calculated to be 46% in EtOH/phosphate-buffered saline 1:1 (10 mM, pH 7.4). The calculated TP action cross-section ($\delta\Phi_f$) was roughly 50 GM at 740 nm (Fig. S2, ESI†). The intensity of the TP excited emission spectra exhibited a linear dependence on the square of the incident laser power, confirming nonlinear absorption (Fig. S2, ESI†). The significant $\delta\Phi_f$ value of **BSe-B** highlights its potential for effective imaging and therapy in deeper tissue layers.[40] We demonstrated the ability of **BSe-B** to generate ROS but not singlet oxygen ($^1O_2$) in PBS buffer (Fig. 1b and c). Each indicator, DHR123 (ROS) and ABDA ($^1O_2$), was mixed with **BSe-B** and irradiated with white light. Consequently, the fluorescence intensity of DHR123, oxidized by the generated ROS, increased.[43] However, since $^1O_2$ was not produced, decomposition of the ABDA absorption spectrum was not observed.[44] Under two-photon irradiation, the PL intensity of DHR123 enhanced significantly, whereas the absorbance of ABDA remains unchanged which demonstrating the type-I ROS production of **BSe-B** (Fig. S3, ESI†). ROS inhibition studies were
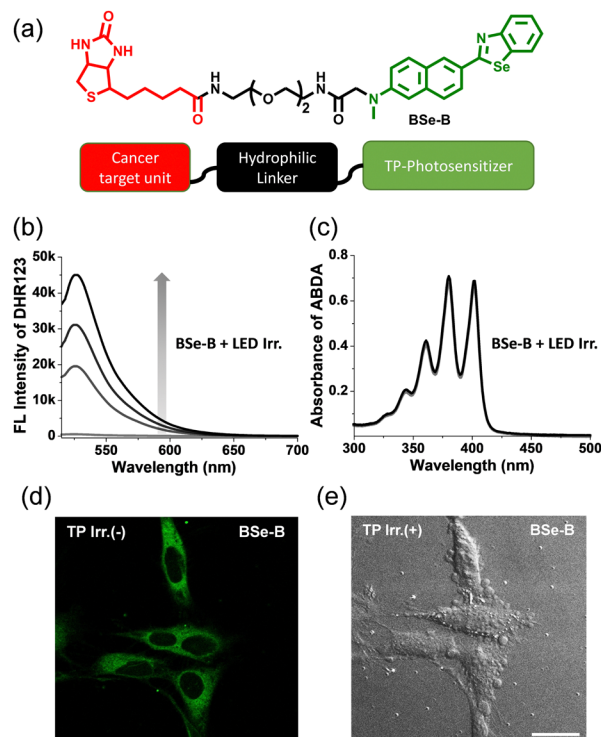

Fig. 1 (a) Chemical structure of **BSe-B**; (b) fluorescence spectra of DHR123 and (c) absorbance spectra of ABDA containing **BSe-B** after white LED irradiation (0–30 min); (d) fluorescence and (e) bright field images of HeLa cells; cells were stained with **BSe-B** (2 μM). After probe staining, cells were irradiated with a two-photon (TP) laser at 730 nm. Excitation: 730 nm; emission: 450–600 nm. Scanning laser: 730 nm; 1.4 mW; 1.3 s per scan; 100 scans. Scale bar: 30 μM.

This journal is © The Royal Society of Chemistry 2024

J. Mater. Chem. B, 2024, **12**, 12232–12238 | **12233**

conducted to confirm the specific ROS produced by **BSe-B** (Fig. S3, ESI†). The results showed that **BSe-B** primarily generates the $O_2^{\bullet-}$ radical and partially produces NOO^- under both white light and two-photon irradiation.

We confirmed the staining ability of **BSe-B** and the effect of TP-PDT on HeLa cells. As shown in Fig. 1d, **BSe-B** is efficiently taken up by HeLa cells, likely due to a specific ligand-receptor-mediated endocytosis process, and it does not form aggregates after being labeled for 30 minutes. Additionally, when the cells were irradiated with a TP laser, the cell-bleb phenomenon was observed, indicating that the cells were damaged (Fig. 1e).[45] **BSe-B** also has the advantage that diagnosis and treatment can be performed simultaneously because its fluorescence intensity allows cell imaging. In short, **BSe-B**, which displayed good ROS generation ability in cuvettes and cells and excellent cell-staining ability, has potential as a PDT tool.

ROS generation and PDT effect of BSe-B in cells

The dark toxicity and phototoxicity of **BSe-B** were evaluated using the CCK-8 assay (Fig. 2a). After incubating HeLa cells with **BSe-B**, the cells were divided into groups irradiated with light or kept in the dark. Cells exposed to light showed a marked decrease in viability, particularly evident at concentrations $\geq 0.2\ \mu M$, demonstrating **BSe-B**'s high phototoxicity with minimal dark toxicity. We assessed the ability of **BSe-B** to induce cell damage *via* ROS generation after TP laser irradiation. ROS generation was evaluated using the dichlorodihydrofluorescein

diacetate (DCHF-DA) assay, in which DCHF-DA, a non-fluorescent compound, enters cells and reacts with ROS to produce fluorescent dichlorofluorescein (DCF).[46] Upon irradiation of HeLa cells with a TP laser in the presence of **BSe-B** and DCHF-DA, a significant increase in DCF fluorescence was observed (Fig. 2b), indicating effective ROS production by **BSe-B**.

Further investigation using ROS and $^1O_2$ scavengers elucidated the mechanism of PDT induced by **BSe-B** (Fig. 2c). HeLa cells treated with **BSe-B** were divided into control, vitamin C (ROS scavenger, 100 μM), or NaN_3 ($^1O_2$ scavenger, 100 μM) groups, followed by propidium iodide (PI) staining to assess cell death.[47,48] In the absence of TP laser irradiation, PI fluorescence indicative of cell death was absent across all groups. Conversely, upon TP laser irradiation, PI fluorescence was observed in the control and NaN_3 groups, whereas the vitamin C group showed no PI fluorescence. This suggests that during PDT, **BSe-B** predominantly operates *via* a type-I mechanism involving ROS generation. These findings underscore **BSe-B**'s efficacy in ROS-mediated PDT and its potential as a targeted cancer therapy.

We conducted cell viability testing using fluorescence-activated cell sorting (Fig. 2d). HeLa cells were divided into a control group stained with dimethylsulfoxide alone or an experimental group stained with **BSe-B** (10 μM). These groups were further subdivided into non-irradiated and TP-irradiated groups. Apoptosis was assessed using Annexin V and PI
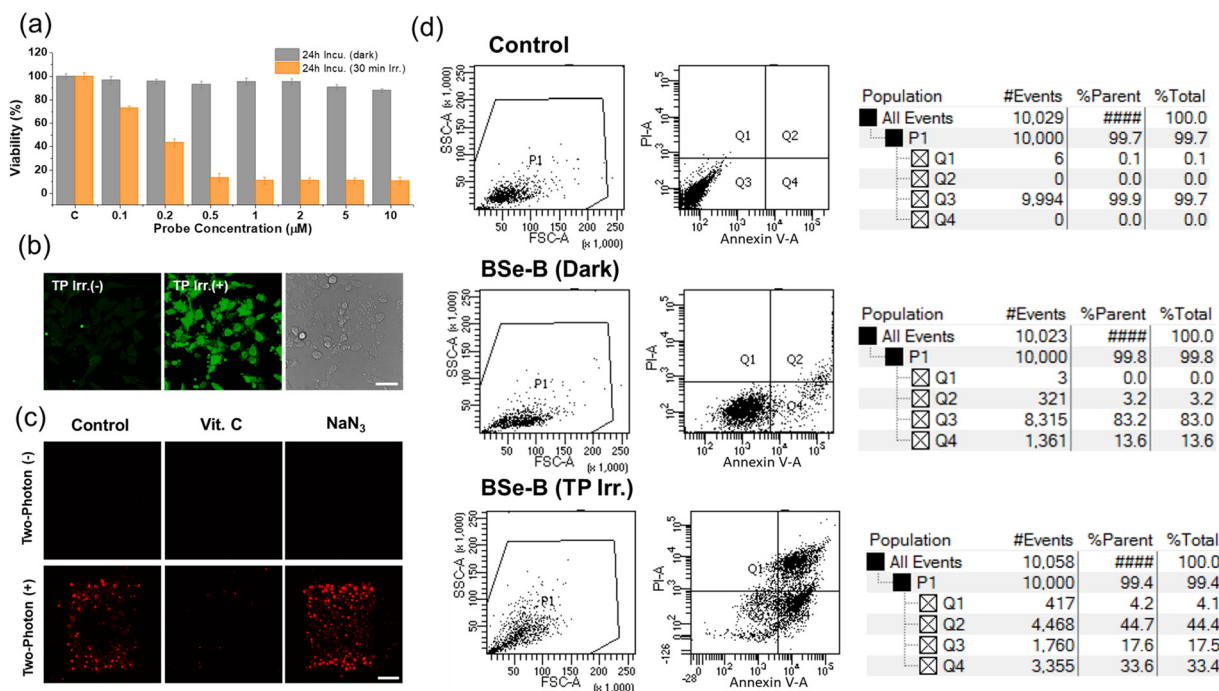

Fig. 2 (a) Viability of HeLa cells after white LED irradiation or non-irradiation; the cells were treated with **BSe-B**. After irradiation, the cells were incubated for 24 h. The viability was measured using CCK-8. (b) Fluorescence images of HeLa cells co-stained with dichlorodihydrofluorescein diacetate (DCHF-DA) (10 μM) and **BSe-B** (2 μM); (c) fluorescence images of HeLa cells treated with **BSe-B** (2 μM), vitamin C (100 μM), or NaN_3 (100 μM). Excitation: 488 nm (DCHF-DA, PI). Emission: 500–550 nm (DCHF-DA), 650–700 nm (PI). Scanning laser: 730 nm, 1.4 mW, 1.3 s per scan, 100 scans. Scale bars: (b) 40 μm and (c) 70 μm. (d) Cell viability of **BSe-B** using FACS analysis in HeLa cells; control (dimethylsulfoxide only), **BSe-B** (10 μM) staining followed by non-irradiation, and TP-irradiation at 730 nm after **BSe-B** (10 μM) staining. After all procedures, the cells were stained with Annexin V and PI (mean ± SD, $n = 3$).

12234 | *J. Mater. Chem. B*, 2024, **12**, 12232–12238

This journal is © The Royal Society of Chemistry 2024

staining.[49–51] The control group showed high cell viability (over 99%), whereas the group stained with **BSe-B** and not irradiated with TP exhibited cell viability of more than 83%. In contrast, TP irradiation led to more than 77% of apoptosis in the **BSe-B** stained group. Additionally, to determine the IC_{50} of **BSe-B** under TP conditions, the live/dead cell ratio was calculated using Hoechst 33342 (live cell indicator) and PI (dead cell indicator).[36,47,52] HeLa cells stained with **BSe-B** at concentrations in the range of 0.2–20 μM were irradiated with a TP laser, revealing an IC_{50} value of approximately 4.9 μM (Fig. S4, ESI†). These findings emphasized the potent apoptotic effect of **BSe-B** under TP irradiation, highlighting its potential as an effective photosensitizer in targeted cancer therapies.

Cancer cell selectivity experiment of BSe-B

The selectivity of **BSe-B** for cancer cells was evaluated using HeLa (biotin-positive cervical cancer) and WI-38 (biotin-negative normal lung) cells (Fig. 3). Following staining with **BSe-B**, real-time monitoring of the two-photon excitation fluorescence (TPEF) intensity was conducted for 60 min in HeLa and WI-38 cells. The fluorescence intensity of **BSe-B** was approximately ten times higher in HeLa cells (cancer cells) compared with WI-38 cells (normal cells) (Fig. 3a and b).

To confirm the specificity of **BSe-B** uptake by cancer cells mediated by the biotin unit, a competition experiment using free biotin was performed.[27,53] Cells treated with free biotin exhibited a fluorescence intensity similar to that of WI-38 cells (Fig. 3a and b), indicating that the enhanced uptake of **BSe-B** in cancer cells could be attributed to the binding between the biotin unit and the overexpressed biotin receptor in the cancer cells.[54] In addition, TP-PDT efficacy experiments were conducted on both cancer and normal cells. After incubating each cell type with **BSe-B** for 1 h, the cells were irradiated with TP according to the number of scans. In HeLa cells, cell death occurred in the TP-irradiated area, whereas no cell death was observed in the WI-38 cells (Fig. 3c). Similar TP-PDT experiments were performed on other cancer cell types, including A549 (lung cancer) and OVCAR-3 (ovarian cancer) cells, where cell death was observed after staining with **BSe-B** and TP irradiation. In contrast, TP irradiation of L-929 cells (normal connective tissue cells) resulted in the death of only a few cells (Fig. S5, ESI†). These results highlight **BSe-B**'s potential for targeted cancer therapy by leveraging biotin-mediated selectivity and TP excitation for precise imaging and treatment.

Biocompatibility test of BSe-B *in vivo*

A biocompatibility experiment was conducted to assess the *in vivo* safety of **BSe-B** (Fig. S6, ESI†). Following injection into mice, the organ morphology was examined using hematoxylin and eosin (H&E) staining (Fig. S6a, ESI†). The results indicated no significant morphological changes compared with the control group, confirming the absence of adverse effects in the organs tested. Biochemical blood analysis further confirmed the absence of toxicity, with no notable differences observed compared with the control group (Fig. S6b, ESI†). Overall, these findings demonstrate that **BSe-B** exhibits excellent biocompatibility, supporting its potential for safe use *in vivo* without compromising liver or kidney function.

TPM imaging in three-dimensional (3D)-spheroid tumor model and human colon tissue

In our major experimental observations, a 3D-spheroid tumor model was used and evaluated (Fig. 4). The fluorescence intensity of **BSe-B** in HeLa cell spheroids was 6 times higher than that of WI-38 cells (Fig. 4a and c). Upon TP irradiation, there was a significant increase in the PI signal, specifically in the HeLa spheroids (Fig. 4b and d), indicating **BSe-B**'s efficacy in targeting and inducing cytotoxicity in HeLa cells.

BSe-B was applied to biopsy samples obtained from patients with colorectal cancer at Ajou University Hospital (Fig. 5). Staining under identical conditions revealed that the TPEF intensity in cancerous tissues was approximately 8 times stronger than that in normal tissues (Fig. 5a and c). This selective uptake was evident not only in two-dimensional cell cultures and 3D spheroids but also in patient-derived colorectal cancer tissues. TP excitation allows the precise targeting of specific regions within tissues. Colorectal cancer tissues treated with **BSe-B** and DHR123 exhibited increased fluorescence (red) of DHR123 solely within the irradiated area marked by a white dotted box (Fig. 5b and d). In contrast, DHR123 fluorescence was not observed in adjacent normal tissues under the same conditions. These results underscore **BSe-B**'s ability to selectively
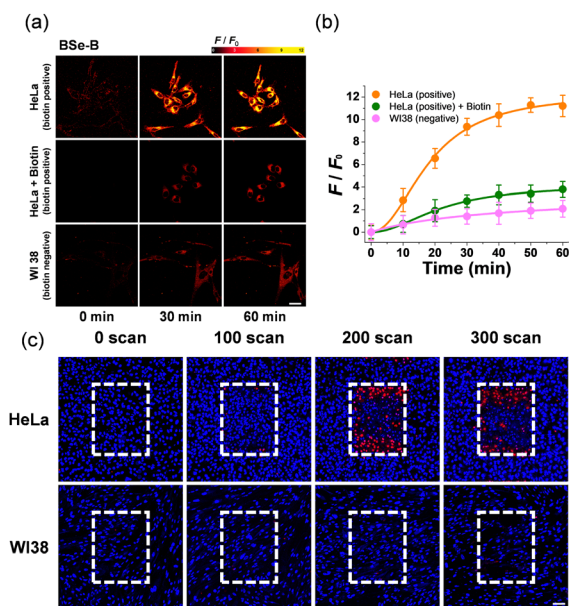

Fig. 3 Biotin-conjugated BSe (**BSe-B**) targeting HeLa cells: (a) real-time TP images of HeLa (biotin-positive) and WI-38 (biotin-negative) cells; cells were treated with **BSe-B** (2 μM) with or without free biotin (1 mM). (b) Relative fluorescence intensities were acquired every 10 min. (c) Fluorescence images of HeLa and WI-38 cells; cells were treated with **BSe-B** (2 μM, 1 h incubation). After probe incubation, TP irradiation was performed within the white-dashed line box areas. Excitation: 488 nm (PI), 730 nm (Hoechst 33342, TP), and 750 nm (**BSe-B**, TP). Emission: 400–450 nm (Hoechst 33342), 480–520 nm (**BSe-B**), and 650–700 nm (PI). Scanning laser: 730 nm, 1.4 mW, 1.3 s per scan. Scale bar: (a) 40 μm, (c) 80 μm (mean ± SD, *n* = 3).

This journal is © The Royal Society of Chemistry 2024

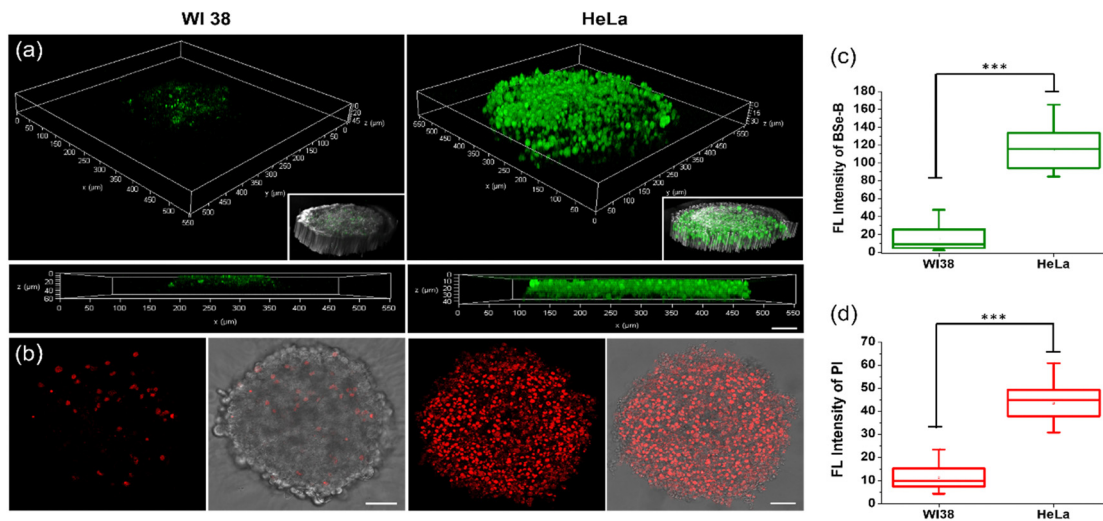*J. Mater. Chem. B*, 2024, **12**, 12232–12238 | **12235**

Fig. 4 Selectivity and toxicity of **BSe-B** towards HeLa spheroids: (a) 3D-spheroid two-photon fluorescence images of HeLa (biotin positive) and WI-38 (biotin negative) cells. Spheroids were stained with **BSe-B** (10 μM) for 3 h. (b) One-photon fluorescence image of PI staining in the spheroid. Spheroids stained with **BSe-B** (10 μM, 3 h incubation) were irradiated with two-photon lasers at 730 nm and then stained with PI (10 μM) for 24 h. (c) Two-photon fluorescence intensity of **BSe-B** in each spheroid; (d) one-photon fluorescence intensity of PI in each spheroid; excitation: 488 nm (PI) and 730 nm (**BSe-B**, TP); emission: 480−520 nm (**BSe-B**) and 650−700 nm (PI); scanning laser: 730 nm, 1.4 mW, 1.3 s per scan. Scale bar: (a) 50 μm, (b) 100 μm (mean ± SD, n = 3), (***p < 0.001).
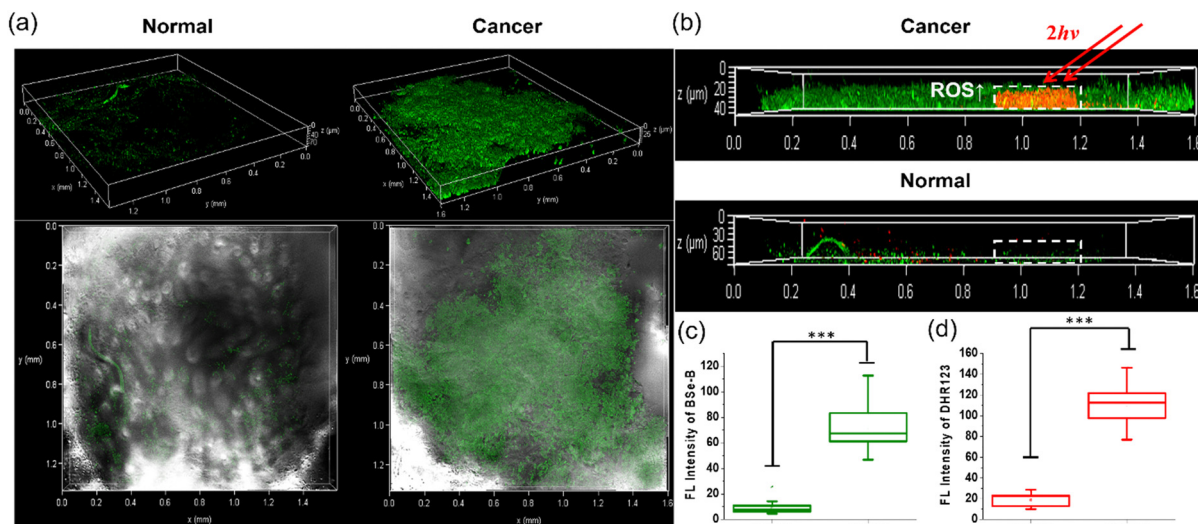

Fig. 5 Selectivity and toxicity of **BSe-B** towards patient-derived colorectal cancer tissues: (a) two-photon 3D images of colon cancer and normal tissues. The tissues were treated with **BSe-B** (10 μM, 3 h incubation). (b) Z-section images of colon tissues after two-photon laser irradiation on the white-dashed line box region; the tissues were treated with **BSe-B** and DHR123. (c) Two-photon fluorescence intensity of **BSe-B** in colon cancer and normal tissues; (d) one-photon fluorescence intensity of DHR123 in colon cancer and normal tissues. Excitation: 488 nm (DHR123, OP), 730 nm (**BSe-B**, TP); emission: 480−520 nm (**BSe-B**), 500−550 nm (DHR123); scanning laser: 730 nm, 1.4 mW, 1.3 s per scan, 100 scans. The images shown in (b) are merges between **BSe-B** (TP, green) and DHR123 (OP, red) (mean ± SD, n = 3), (***p < 0.001).

target and induce cytotoxic effects within distinct regions of colorectal cancer tissue *ex vivo*, highlighting its potential as a promising therapeutic strategy for future applications.

Conclusions

We developed and synthesized **BSe-B**, a two-photon photodynamic therapy (TP-PDT) probe engineered for selective cancer targeting. By conjugating a biotin unit to BSe, known for its potent ROS generation, **BSe-B** was tailored to possess superior ROS generation capability, minimal dark toxicity, excellent cell-staining ability, and remarkable cancer selectivity. This biocompatible probe effectively differentiated cancer cells (HeLa, A549, and OVCAR-3) from normal cells (WI-38, L-929) across diverse cell lines, demonstrating significant therapeutic potential. **BSe-B** *in vivo* revealed no significant morphological

12236 | *J. Mater. Chem. B*, 2024, **12**, 12232–12238

This journal is © The Royal Society of Chemistry 2024

changes or biochemical abnormalities in the organs. Furthermore, **BSe-B** precisely discriminated between cancerous and normal tissues in 3D-spheroid models and live human colon tissue samples. Under TP laser irradiation, which offers spatial selectivity, **BSe-B** induces cell death and ROS generation deep within the tissues. This capability underscores **BSe-B**'s potential as an advanced TP-PDT tool capable of integrating imaging-guided therapy, enabling precise treatment and facilitating the assessment of therapeutic outcomes.

Author contributions

Dong Joon Lee: investigation, writing – original draft; Vinayak Juvekar: investigation, writing – original draft; Yu Cao: investigation, data curation; Sauraj: investigation, data curation; Choong-Kyun Noh: investigation; Sung Jae Shin: conceptualization; Zhihong Liu: data curation, writing – review, and editing; Hwan Myung Kim: supervision; conceptualization; writing – review & editing.

Data availability

The data supporting this article have been included as part of the ESI.†

Conflicts of interest

There are no conflicts to declare.

Acknowledgements

References

1 A. Kawczyk-Krupka, A. M. Bugaj, W. Latos, K. Zaremba, K. Wawrzyniec, M. Kucharzewski and A. Sieron, *Photodiagn. Photodyn. Ther.*, 2016, **13**, 158–174.

2 C. Hopper, *Lancet Oncol.*, 2000, **1**, 212–219.

3 N. P. Brodin, C. Guha and W. A. Tome, *Technol. Cancer Res. Treat.*, 2015, **14**, 355–368.

4 P. Agostinis, K. Berg, K. A. Cengel, T. H. Foster, A. W. Girotti, S. O. Gollnick, S. M. Hahn, M. R. Hamblin, A. Juzeniene, D. Kessel, M. Korbelik, J. Moan, P. Mroz, D. Nowis, J. Piette, B. C. Wilson and J. Golab, *CA Cancer J. Clin.*, 2011, **61**, 250–281.

5 D. E. Dolmans, D. Fukumura and R. K. Jain, *Nat. Rev. Cancer*, 2003, **3**, 380–387.

6 M. C. DeRosa and R. J. Crutchley, *Coord. Chem. Rev.*, 2002, **233**, 351–371.

7 P. Mroz, A. Yaroslavsky, G. B. Kharkwal and M. R. Hamblin, *Cancers*, 2011, **3**, 2516–2539.

8 K. Plaetzer, T. Kiesslich, T. Verwanger and B. Krammer, *Med. Laser Appl.*, 2003, **18**, 7–19.

9 D. Van Straten, V. Mashayekhi, H. S. De Bruijn, S. Oliveira and D. J. Robinson, *Cancers*, 2017, **9**, 19.

10 Z. Zhou, J. Song, L. Nie and X. Chen, *Chem. Soc. Rev.*, 2016, **45**, 6597–6626.

11 H. Abrahamse and M. R. Hamblin, *Biochem. J.*, 2016, **473**, 347–364.

12 F. Hu, S. Xu and B. Liu, *Adv. Mater.*, 2018, **30**, e1801350.

13 M. R. Detty, S. L. Gibson and S. J. Wagner, *J. Med. Chem.*, 2004, **47**, 3897–3915.

14 J. Chen, T. Fan, Z. Xie, Q. Zeng, P. Xue, T. Zheng, Y. Chen, X. Luo and H. Zhang, *Biomaterials*, 2020, **237**, 119827.

15 L. Bretin, A. Pinon, S. Bouramtane, C. Ouk, L. Richard, M. L. Perrin, A. Chaunavel, C. Carrion, F. Bregier, V. Sol, V. Chaleix, D. Y. Leger and B. Liagre, *Cancers*, 2019, **11**, 1474.

16 L. Bildstein, C. Dubernet and P. Couvreur, *Adv. Drug Delivery Rev.*, 2011, **63**, 3–23.

17 Y. Singh, M. Palombo and P. J. Sinko, *Curr. Med. Chem.*, 2008, **15**, 1802–1826.

18 M. J. Akhtar, M. Ahamed, H. A. Alhadlaq, S. A. Alrokayan and S. Kumar, *Clin. Chim. Acta*, 2014, **436**, 78–92.

19 G. Russell-Jones, K. McTavish, J. McEwan, J. Rice and D. Nowotnik, *J. Inorg. Biochem.*, 2004, **98**, 1625–1633.

20 S. Chen, X. Zhao, J. Chen, J. Chen, L. Kuznetsova, S. S. Wong and I. Ojima, *Bioconjug. Chem.*, 2010, **21**, 979–987.

21 A. D. Vadlapudi, R. K. Vadlapatla, D. Pal and A. K. Mitra, *Int. J. Pharm.*, 2013, **441**, 535–543.

22 K. Li, L. Qiu, Q. Liu, G. Lv, X. Zhao, S. Wang and J. Lin, *J. Photochem. Photobiol., B*, 2017, **174**, 243–250.

23 Y. Singh, K. K. Durga Rao Viswanadham, A. Kumar Jajoriya, J. G. Meher, K. Raval, S. Jaiswal, J. Dewangan, H. K. Bora, S. K. Rath, J. Lal, D. P. Mishra and M. K. Chourasia, *Mol. Pharm.*, 2017, **14**, 2749–2765.

24 N. U. Deshpande and M. Jayakannan, *Biomacromolecules*, 2018, **19**, 3572–3585.

25 M. F. Isaac-Lam and D. M. Hammonds, *Pharmaceuticals*, 2017, **10**, 41.

26 P. Balçik-Erçin, M. Çetin, M. Göksel and M. Durmuş, *New J. Chem.*, 2020, **44**, 3392–3401.

27 D. J. Lee, V. Juvekar, H. W. Lee, E. S. Kim, C. K. Noh, S. J. Shin and H. M. Kim, *Anal. Chem.*, 2021, **93**, 16821–16827.

28 T. Dai, Y. Y. Huang and M. R. Hamblin, *Photodiagn. Photodyn. Ther.*, 2009, **6**, 170–188.

29 W. R. Zipfel, R. M. Williams and W. W. Webb, *Nat. Biotechnol.*, 2003, **21**, 1369–1377.

30 F. Helmchen and W. Denk, *Nat. Methods*, 2005, **2**, 932–940.

31 R. M. Williams, W. R. Zipfel and W. W. Webb, *Curr. Opin. Chem. Biol.*, 2001, **5**, 603–608.

32 C. Xu, W. Zipfel, J. B. Shear, R. M. Williams and W. W. Webb, *Proc. Natl. Acad. Sci. U. S. A.*, 1996, **93**, 10763–10768.

33 M. Göppert-Mayer, *Ann. Phys.*, 1931, **401**, 273–294.

34 W. Kaiser and C. G. B. Garrett, *Phys. Rev. Lett.*, 1961, **7**, 229–231.

This journal is © The Royal Society of Chemistry 2024

J. Mater. Chem. B, 2024, **12**, 12232–12238 | **12237**

35 J. D. Bhawalkar, N. D. Kumar, C. F. Zhao and P. N. Prasad, *J. Clin. Laser Med. Surg.*, 1997, **15**, 201–204.

36 V. Juvekar, C. S. Lim, D. J. Lee, S. J. Park, G. O. Song, H. Kang and H. M. Kim, *Chem. Sci.*, 2021, **12**, 427–434.

37 Y. X. Li, D. T. Xie, Y. X. Yang, Z. Chen, W. Y. Guo and W. C. Yang, *Molecules*, 2022, **27**, 4501.

38 R. Tian, W. Sun, M. Li, S. Long, M. Li, J. Fan, L. Guo and X. Peng, *Chem. Sci.*, 2019, **10**, 10106–10112.

39 M. Lan, S. Zhao, W. Liu, C. S. Lee, W. Zhang and P. Wang, *Adv. Healthcare Mater.*, 2019, **8**, e1900132.

40 V. Juvekar, H. W. Lee, D. J. Lee and H. M. Kim, *TrAC-Trends Anal. Chem.*, 2022, **157**, 116787.

41 W. X. Ren, J. Y. Han, S. Uhm, Y. J. Jang, C. Kang, J. H. Kim and J. S. Kim, *Chem. Commun.*, 2015, **51**, 10403–10418.

42 S. Maiti, N. Park, J. H. Han, H. M. Jeon, J. H. Lee, S. Bhuniya, C. Kang and J. S. Kim, *J. Am. Chem. Soc.*, 2013, **135**, 4567–4572.

43 F. A. Villamena, Fluorescence Technique, in *Reactive Species Detection in Biology*, ed. F. A. Villamena, Elsevier, 2017, pp. 87–162.

44 T. Entradas, S. Waldron and M. Volk, *J. Photochem. Photobiol., B*, 2020, **204**, 111787.

45 J. W. Mills, M. Horster and P. Wilson, *Cell Biol. Int. Rep.*, 1986, **10**, 11–17.

46 D. Yu, Y. Zha, Z. Zhong, Y. Ruan, Z. Li, L. Sun and S. Hou, *Sens. Actuators, B*, 2021, **339**, 129878.

47 I. Nicoletti, G. Migliorati, M. C. Pagliacci, F. Grignani and C. Riccardi, *J. Immunol. Methods*, 1991, **139**, 271–279.

48 S. Wang, W. Wu, P. Manghnani, S. Xu, Y. Wang, C. C. Goh, L. G. Ng and B. Liu, *ACS Nano*, 2019, **13**, 3095–3105.

49 M. Van Engeland, L. J. Nieland, F. C. Ramaekers, B. Schutte and C. P. Reutelingsperger, *Cytometry*, 1998, **31**, 1–9.

50 A. P. Demchenko, *Cytotechnology*, 2013, **65**, 157–172.

51 A. M. Rieger, K. L. Nelson, J. D. Konowalchuk and D. R. Barreda, *J. Vis. Exp.*, 2011, **50**, e2597.

52 B. Chazotte, *Cold Spring Harb. Protoc.*, 2011, pdbprot5557.

53 M. Ren, Q. Xu, S. Wang, L. Liu and F. Kong, *Chem. Commun.*, 2020, **56**, 13351–13354.

54 O. Tredan, C. M. Galmarini, K. Patel and I. F. Tannock, *J. Nat. Cancer Inst.*, 2007, **99**, 1441–1454.

12238 | *J. Mater. Chem. B*, 2024, **12**, 12232–12238

This journal is © The Royal Society of Chemistry 2024